Analysis of Specific Events on the Deformation Curves under MgO Nano-/Microindentation

Olga Shikimaka[a], Daria Grabco[a], Constantin Pyrtsac[a,b], Andrian Prisacaru[a,b], Alexandru Bordei[c]

[a] Institute of Applied Physics, Moldova State University, Chisinau, MD-2028, Moldova Republic
[b] Tehnical University of Moldova, Chisinau, MD-2045, Moldova Republic
[c] Orizont Theoretical Lyceum, Chisinau, MD-2003, Moldova Republic

Abstract: Specific features on the *P-h* curves known as pop-in and pop-out events, were studied using the depth-sensing nano-/microindentation of the (001) plane of MgO single crystals. The sharp (*with* pop-in) and gradual (*without* pop-in) mechanisms of elastic-to-plastic transition were revealed and the conditions of their appearance were analyzed. Three types of pop-in jumps were identified, and the correlation of each of them with the shape of dislocation rosettes around the imprints was established. It was shown that pop-in jumps are caused by different mechanisms of plastic deformation and pop-out jumps are the result of a sharp stress relaxation by cracks generation during the load removal stage.

Keywords: MgO single crystal, nanoindentation, deformation speed, strain rate, pop-in effect, pop-out effect, dislocation structure.

Introduction

The pop-in effect is one of the interesting phenomena revealed under the depth-sensing indentation of crystalline materials representing a step-wise jump, registered on the loading part of nanoindentation curve, caused by instantaneous penetration of the indenter into the material. The pop-in event takes place in a material when the stresses underneath the indenter reach the values corresponding to the theoretical strength of the material and denotes the transition from pure elastic to elastic-plastic deformation.

The pop-in effects were investigated on a range of crystalline materials from superhard ceramics (Al_2O_3, SiC) to soft metals (Cu, Al) and were attributed to the dislocations nucleation in defect free zones of material [1-18]. It was shown that the pop-in occurrence is more probable for smaller tip radii of the indenter and lower initial density of dislocations in the stressed zone [4]. The pop-in events were successfully obtained by sharp Berkovich and cube-corner indenters with the tip radii of the order of 100-200 nm [5], as well as by 9.5 μm spherical indenter using a special technique for surface preparation [6]. In some works the pop-in was syudied by comparing the theoretical estimates of molecular dynamics (MD) simulation of nanoindentation with the experimental data of the *P-h* or *H-h* curves shape [14,18,19]. Thus, based on the Gao-Nix model [20] about the geometrically necessary dislocations (GNDs), Durst and colleagues [14] modeled the indentation process and obtained good agreement with the experimental load-displacement data on a number of metals: Cu, Ni, Al, W. They identified three stages of the deformation process: (i) the elastic stage, (ii) the stage that begins immediately after the

pop-in effect, in which the GNDs dominate, and (iii) further the plastic deformation is controlled by GND and statistically stored dislocations (SSDs). Bradby *et al* found a linear dependence between the pop-in load, the extention of pop-in jump and the hardness for a range of semiconductors (GaN, GaAs, InP and ZnO) [7].

Some crystals demonstrate several pop-in jumps [13,14,23]. For example, under bulk Al indentation, Ohmura *et al* [13] observed (along with a clear first pop-in jump at a load of 0.05 mN) many smaller pop-in effects with further loading of the sample to 0.25 mN, but the reasons for their occurrence were not discussed. The staircase yielding representing also the a sequence of pop-in events has been detected on Al under indentation with 200 μN load [14] and was explained within the framework of the concept of GNDs and SSDs. In our earlier work the peculiarities of the deformation of LiF single crystals under nanoindentation in the large interval of loads P= (2÷900) mN were investigated [23]. A comparison of the *P-h* curves with the shape of dislocation rosettes appearing around the imprints demonstrated a clear correlation between the appearance of the first pop-in effect, as well as additional pop-in steps, with the growth of load and sequential development of various dislocation processes. Taking into account that the LiF crystal has a relatively low hardness (H =1.2 GPa), ionic type of bonding and high dislocation velocity at the room temperature (v_{LiF} =10^{-5}÷10^{0}cm/s), it was of interest to consider if such a correlation will occur under the indentation of the MgO crystal having higher hardness (H =8.0 GPa), ion-covalent type of bond and much lower dislocation velocity (v_{MgO} = 10^{-6} ÷ 10^{-2} cm/s).

It is known that the

Experimental

The (001) face of a freshly cleaved MgO single crystal, (10x10x2) mm in size (with no further processing), was subjected to the depth-sensing hardness measurements at the room temperature using the Nanotester-PMT3-NI-02 equipped with a Berkovich indenter.

In order to follow the evolution of the development of the indentation process with the increase in loading, the tests were carried out at 18 values of the peak load in the range P_{max} = (2÷900) mN, according to the following pattern: a load stage of 20 s, holding at a peak load for 5 s, and unloading for 20 s; 5 indentations were made for each load value. Using the *P-h* dependence, the values of Young's modulus and hardness were determined for each imprint in accordance with the Oliver-Pharr method [25,26]. It was found that the Young's modulus value for MgO was ≈250 GPa. According to the obtained results there was constructed a *P-h* diagram that governs the loading/unloading process and the hardness H according to the applied load. The processes of the plastic deformation of the investigated material were evaluated on the basis of the analysis of the indentation curves and dislocation rosettes around the imprints.

The research of the microstructure of the deformed regions around the imprints was carried out using light microscopy (LM) with the help of XJL-101 and Amplival reflection microscopes and a MII-4 interference microscope. The atomic force microscopy (AFM, Nanostation II) was used to study the relief and microstructure of the deformed zone of the imprints at low loads P_{max} = (7÷40) mN. The dislocation rosettes around the indentations were detected with the selective chemical etching in a solution with the following composition: 5p NH_4Cl + 1p H_2O + 1p H_2SO_4.

Results and discussion

The representative *P-h* curves for each of the used 18 loads are presented in Fig. 1. The occurrence of three pop-in jumps at the initial stages of loading is clearly visible being most pronounced for low peak loads (P_{max} = (2÷40) mN). Usually, the pop-in effect at the initial stages of indenter penetration in crystalline materials is associated with homogenous dislocation nucleation and the transition from elastic to plastic deformation [21,27]. As a result, a sudden drop of stresses and a simultaneous sharp increase of the penetration depth take place, exhibited as a pop-in jump on the *P-h* curves.

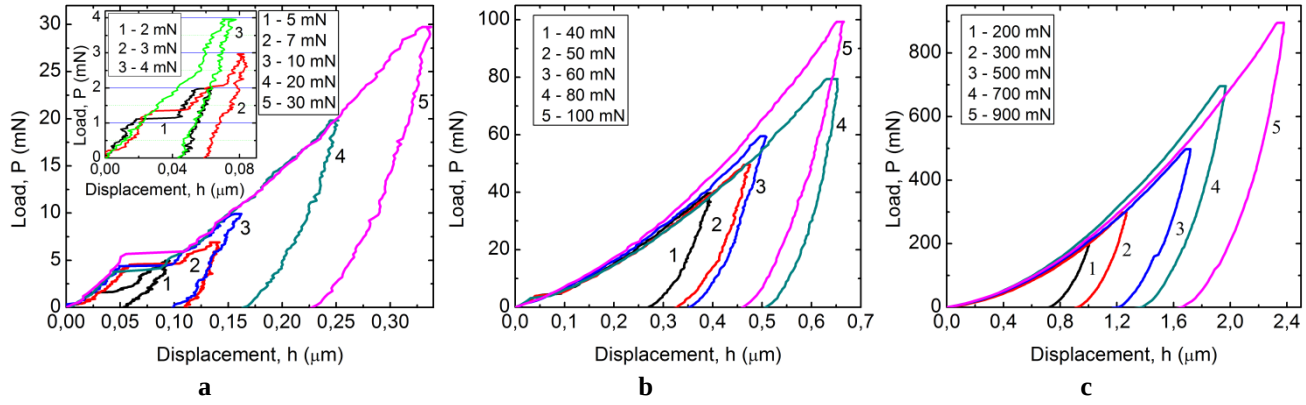

Fig. 1 Loading-unloading diagrams*P(h)* obtained at different peak loads, P_{max}=2÷900 mN

With a further increase in the load, slight oscillations or "stepped appearance" are observed on the deformation curves both at the stage of loading and at the stage of unloading (serration effect). Presumably, this effect is due to the elastic-plastic recovery (relaxation) of the material that takes place throughout the whole process of indentation [28-36]. The serration of the curves decreases at high loads and the *P(h)* dependences become more homogeneous. Let us analyze in more detail the *P-h* diagrams presented in Fig. 2 for 7 loads (P_{max} = 3, 10, 20, 50, 80, 200, and 500 mN), selected from

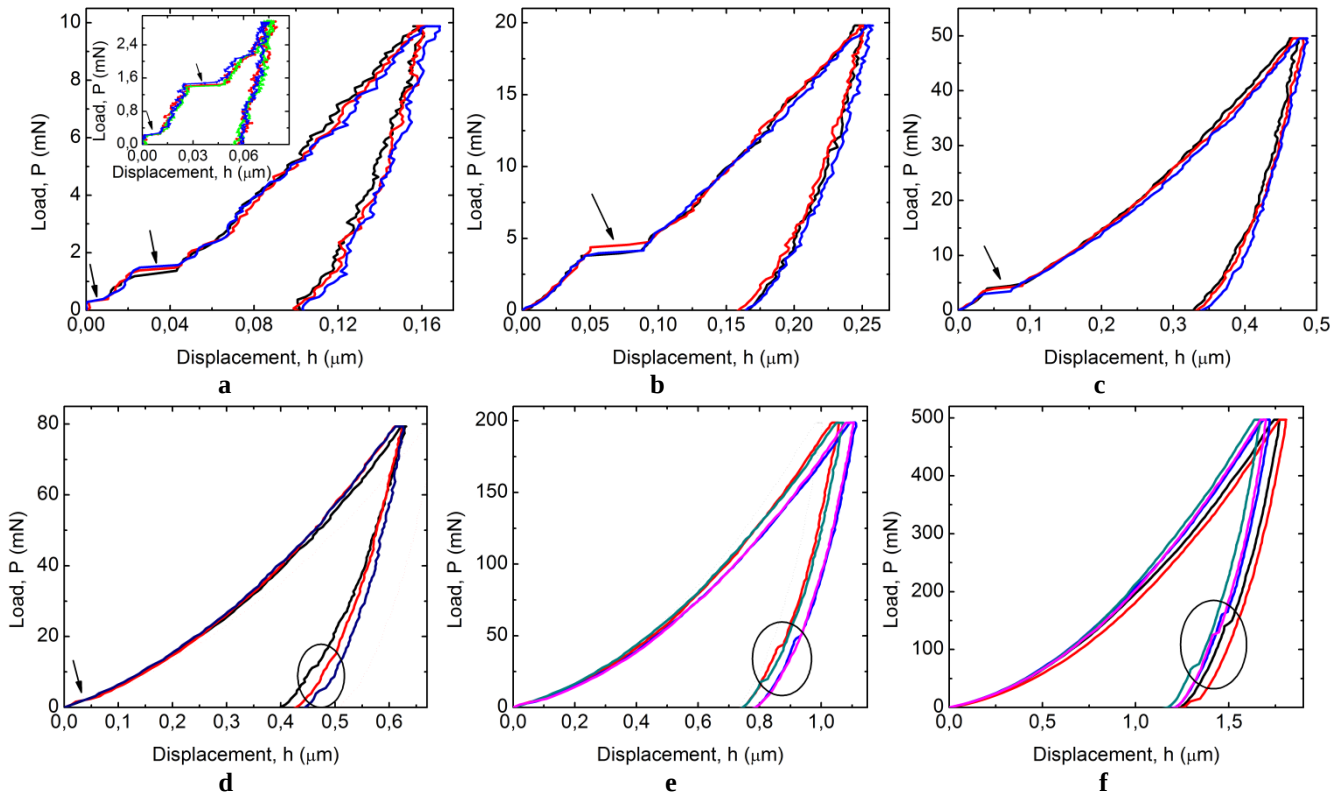

Fig. 2 Loading-unloading diagrams *P(h)* obtained at different peak loads, P_{max}=3 (in the insert),10, 20, 50, 80, 200, and 900 mN. The arrows indicate the "pop-in" phenomena at the loading stage, and the circles indicate the "pop-out" effects at the unloading one

all the 18 studied ones, to find out the nature of the above mentioned evolution of the indentation process.

The following features can be identified from the analysis of the loading-unloading curves. Two pop-in effects are clearly distinguished in the *P-h* diagrams in the range of the load values P_{max} = (3÷10) mN. The first pop-in jump starts from a load of $P_i \approx$ (0.2÷0.3) mN, with the depth of the indenter penetration about $h_i \approx$ 10 nm (Fig. 2a, the insert). The second pop-in jump occurs in the load interval of $P_i \approx$ (1.4÷1.7) mN, for which the penetration depth is $h_i \approx$ (25÷30) nm (Fig. 2a). The first two pop-in discontinuities decrease in size and almost disappear as the value of P_{max} increases in the interval (20÷100) mN. They are replaced by the third jump at $P_i \approx$ 5 mN, corresponding to the depth of indentation $h_i \approx$ (50÷60) nm (Fig. 2b-f). At greater loads, P_{max} = (200÷900) mN, the pop-in steps are hardly visible and finally disappear in general on the *P(h)* diagrams. The pop-out jumps appear on the *P(h)* curves at the unloading stage at P_{max}= (80÷900) mN, may be associated with the formation of cracks around the indentations during the removal of the indenter [37,38].

In our experiments, for all peak loads we used the same indentation time scheme (t_1-t_2-t_3) = (20-5-20) s, where t_1 is loading time, t_2 is holding time under P_{max} and t_3 is unloading time. This fact leads to a sharp increase of the loading rate ($v_p = P_{max}/t_1$) with the increase of peak load (Table 1). As follows from the table, an enhancement in P_{max} from 2 mN to 900 mN increases v_p by a factor of 450, i.e., by 2.5

orders of magnitude. This in turn leads to the increase of the indenter displacement rate, and hence, to the increase of the rate of the deformation of material. Fig. 3 demonstrates the changes of the deformation rate (*dh/dt*) with penetration depth during loading for indentations made with different loads and loading rates according to Table 1. The increase of peak load and, respectively loading rate (in our particular case) leads to a strong increase of the deformation rate, especially at the beginning of indenter penetration (Fig. 3a, b). For higher loads and loading rates the deformation rate decreases considerably with the increase of penetration depth (Fig. 3b), but higher deformation rate for higher loading rate is anyway maintained for any penetration depth. The surges on the *dh/dt(h)* curves 1–4 appear due to a sharp increase of the strain rate during the pop-ins.

Table 1 The change of the loading-unloading rate (v_p) with the increase of P_{max} using the same indentation time regime (20-5-20) s

P_{max}, mN	2	3	4	5	7	10	20	30	40	50	60	80	100	200	300	500	700	900
v_p, mN/s	0.1	0.15	0.2	0.25	0.35	0.5	1.0	1.5	2.0	2.5	3.0	4.0	5.0	10.0	15.0	25.0	35.0	45.0

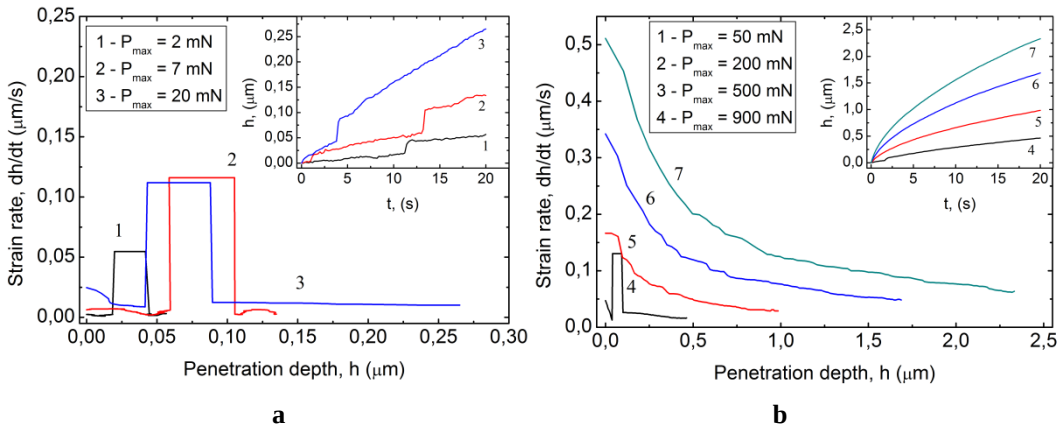

a **b**

Fig. 3 The change of strain rate during loading with the increase of peak load P_{max} and loading rate v_p, according to Table 1

At the same time the use of an identical indentation time scheme for all peak loads induces some specificity in the registration of indentation process. The initial portions of the *P-h* curves for 9 values of P_{max} are shown in Fig. 4. It can be seen that the number of points recorded by the instrument is considerably different when passing from low values of P_{max} to high ones.

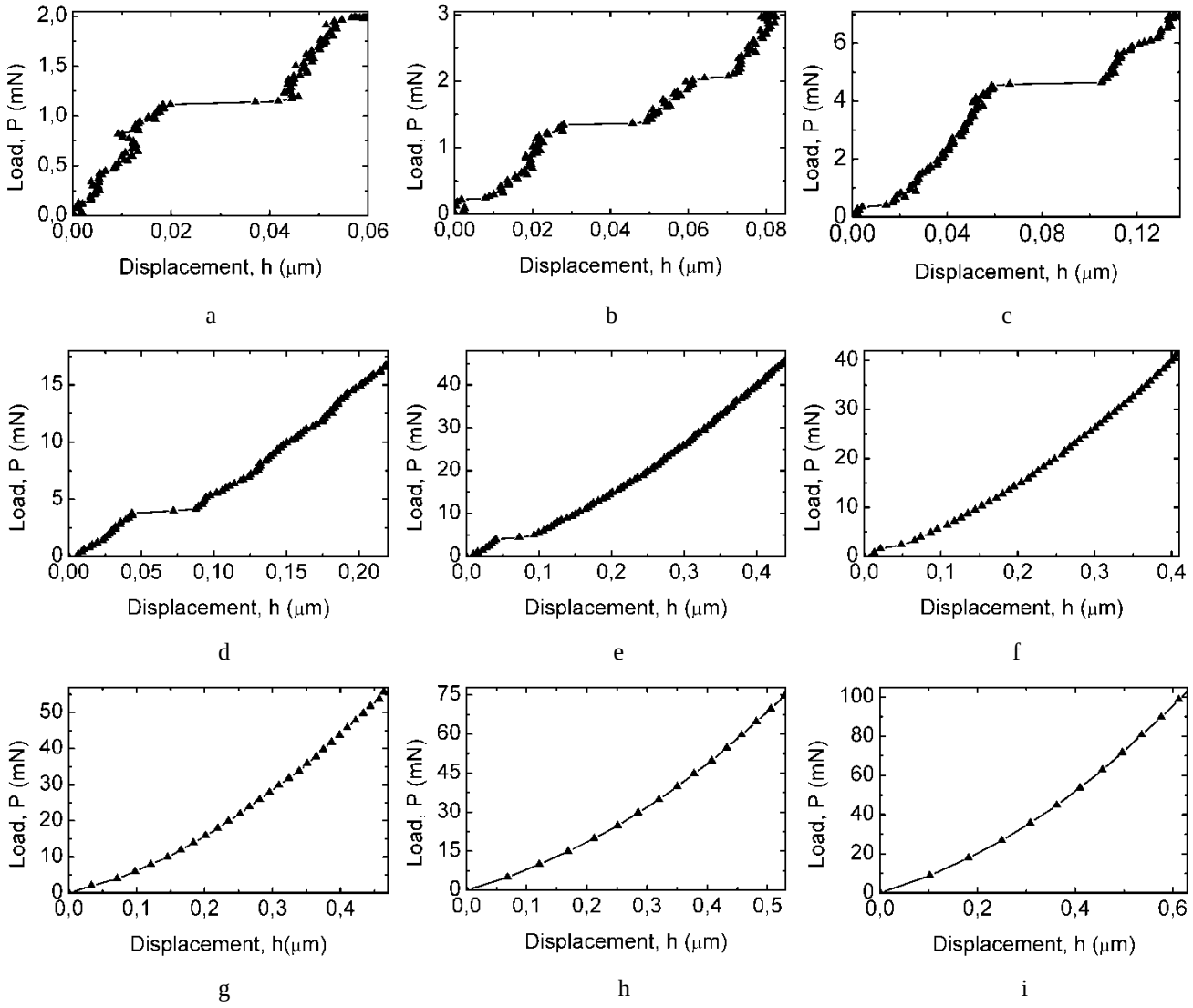

Fig. 4 The shape of the *P-h* diagrams at the initial loading stage for various P_{max}, mN: a – 2; b – 3; c – 7; d – 20; e – 50; f – 80; g – 200; h – 500; i – 900

The averaged time resolution of the instrument is 0.2 s, hence for the same loading-unloading time, $t_1 = t_3 = 20$ s, the spatial resolution changes from $\Delta h \approx 0.75$ nm for 20 mN indentations with maximum depth (h_{max}) of ~75 nm, to $\Delta h \approx 24$ nm for 900 mN indentations with h_{max} of ~2400 nm. As a result, one can assume that it is less possible to "capture" subtler effects on the *P-h* diagrams, such as pop-in jumps and serration, when the values of Δh become close to the depth of pop-in jumps $\Delta h_{p-i} \approx$ (20-50) nm.

To verify the influence of the above mention technical feature we carried out 100 mN indentation using another time regime (200-5-200) s to obtain higher spatial resolution and compare the obtained *P-h* curves with those obtained for (20-5-20) s regime and the same 100 mN load (Fig. 5). As one can see, h_{max} is ~700 nm for both regimes and hence $\Delta h \approx 0.7$ nm for (200-5-200) s regime (Fig. 5a), whereas $\Delta h \approx 7$ nm for (20-5-20) s one (Fig. 5b). The value Δh of even 7 nm is several time lower than that of the mean depth of pop-in jump $\Delta h_{p-i} = 47$nm, well distinguished on the *P-h* curves for (200-5-200) s regime (Fig. 5a), that means that from technical point of view both regimes can equally visualize the pop-in effects. But really, the (200-5-200) s regime exhibits well pronounced pop-ins in four of five case (Fig.

5a), whereas the regime (20-5-20) s displays a pop-in in only one of five case and even this one has a less sharp, gradual aspect (Fig. 5b). This denotes another reason for such a behavior, most probably the different loading rate – 0.5 mN/s demonstrating a higher probability of pop-in formation versus 5 mN/s with lower probability of pop-in formation.

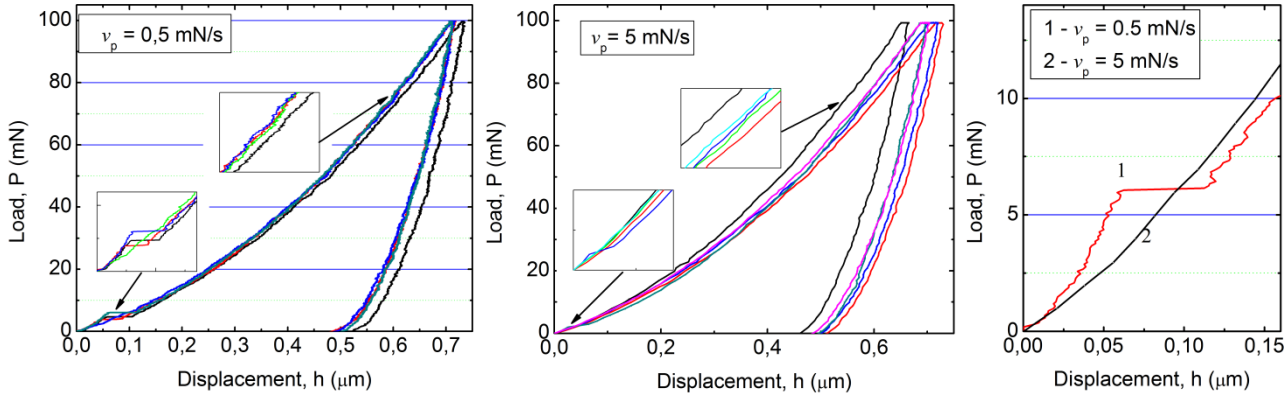

Fig. 5 The *P(h)* diagrams obtained at different loading-unloading rate *v*, mN/s: a – 0.5; b – 5. The inserts show the sections of the curves with a larger magnification (marked by arrows). c – the initial parts of the representative curves from a and b

As mentioned above, the pop-in effect is caused by homogenous dislocation nucleation associated with the transition from elastic to plastic deformation. This process begins when the shear stresses beneath the indenter attain critical values necessary for the dislocation nucleation and sliding. From the classical Hertzian analysis and the Tresca criterion the maximum shear stresses τ_{max} beneath a spherical indenter can be expressed as a function of the mean contact pressure p_m [21, 39,]:

$$\tau_{max} = 0.465 p_m \qquad (1).$$

The mean contact pressure created by the indenter presents the instantaneous hardness during the deformation that follows directly from the definition of the hardness:

$$p_m = P/A \qquad (2),$$

where P is load and A is the contact area.

For Berkovich indenter, as well as for spherical one, τ_{max} is also directly proportional to p_m. Therefore, according to equations (1) and (2), for the indentations made with the same P_{max} = 100 mN, as in the case discussed above, the created τ_{max} should also have the same value, hence the different behavior of the elastic-to-plastic transition is influenced by different loading rate and the induced strain rate. Similar to Fig. 3, Fig 6 shows that higher loading rate induces higher strain rate of the material.

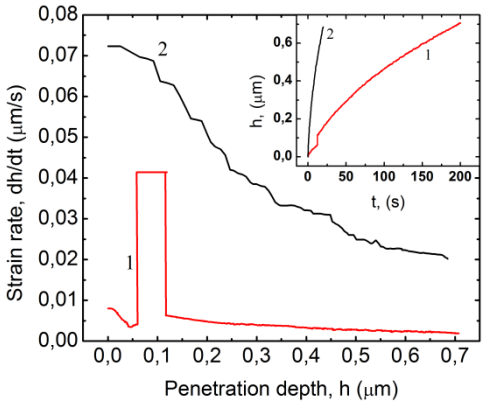

Fig. 6 The change of strain rate during loading for 100 mN indentations made at loading rate of 5 mN/s (curve 1) and 0.5 mN/s (curve 2). Inserted are the respective *h(t)* dependences

The equation introduced by E. Orowan [40] describes the relation between the macroscopic plastic strain rate of the material $\dot{h} = dh/dt$ and the mean velocity of dislocations $\bar{v}$:

$$\dot{h} = \rho_d b \bar{v} \qquad (3),$$

where ρ_d is the density of moving dislocations and b is the Burgers vector.

It is known that dislocation velocity is a function of τ and temperature of deformation (T), but as follows from equation (23) the dislocation velocity also depends on the macroscopic strain rate induced by loading rate. To accommodate to higher loading rate and strain rate at other equal conditions (τ, ρ_m, T), the velocity of dislocation movement must increase. According to the known formula, dislocations of higher velocities have higher kinetic energy [41]:

$$E_d = \frac{E_0}{\sqrt{1-\frac{v^2}{c^2}}} \qquad (4),$$

where E_0 is the energy of stationary dislocation, v is the velocity of dislocation and c is the velocity of sound in material.

The motion of dislocations in crystals requires to overcome various kinds of potential barriers related to both the periodic structure of the crystal (the Peierls barriers) and the lattice defects [42,43]. „Fast" dislocations of higher energies generated at higher strain rate overcome easier these barriers, as opposed to „slow" dislocations generated at lower strain rate, which need higher internal stresses to overcome the barriers. It is clearly seen on Fig. 5c that the curve for 0.5 mN/s demonstrates an increase of P just before the pop-in, as distinct from curve for 5 mN/s that does not contain any pop-in. As the internal stresses depend on the mean contact pressure at the indenter-material interface (Formula 1), it is reasonable to compare the contact pressures instead of P for these two cases.

Basing on the Oliver-Pharr method [25], Novikov et al [44] proposed a technique, which allows determining the contact pressure p_m during indentation process at any penetration depth from *P(h)* dependences, assuming that h_s is directly proportional to the square root of the load P:

$$\frac{h_{s(i)}}{h_{s(\max)}} = \left(\frac{P_i}{P_{\max}} \right)^{\frac{1}{2}} \qquad (5),$$

where $h_{s(i)}$, $h_{c(i)} = h - h_{s(i)}$ and P_i are, respectively, the elastic bending of the sample surface, the contact depth and load in point „*i*" of the $P(h)$ curve. Knowing $h_{s(i)}$, $h_{c(i)}$ in any point of the *P(h)* curve can be determined, which allows the estimation of $p_{c(i)}$ at any penetration depth:

$$p_{c(i)} = \frac{P_i}{A(h_{c(i)})} \qquad (6),$$

where $A(h_{c(i)})$ is the projected area at the contact depth $h_{c(i)}$.

Using this technique, the $p_m(h)$ dependences during loading for two cases mentioned above were obtained (Fig. 7). For the indentation with pop-in made at lower loading rate (0.5 mN/s) and strain rate, the contact pressure p_m demonstrates a sharp increase before the the pop-in as a result of the internal stresses increase, necessary to move „slow" dislocations. Whereas for higher loading rate (5 mN/s), the $p_m(h)$ curve demonstrates much lower values of p_m at the beginning of indenter penetration, which decrease gradually, as „fast" dislocations have initially higher kinetic energy and begin to slide at lower stresses. The same evolution of $p_m(h)$ curves that has the same reason, is observed with the increase of P_{max} and strain rate: the $p_m(h)$ curves corresponding to the indentation process of relatively low strain rates and therefore containing pop-ins, exhibit a considerable increase of p_m before the pop-in (Fig. 8).

This results demonstrates that higer loading and strain rates cause the generation of dislocations of higher velocity and kinetic energy able to overcome the barriers under lower shear stresses and in this case the transition from elastic to plastic deformation is gradual. For lower loading and strain rates the transition mechanism is different: the dislocations of initially lower velocity and energy need an increase of stresses (confirmed by the calculation of p_m) till the critical ones to gain sufficient energy, after which a bulk burst of dislocations takes place causing a pop-in jump and, respectively, a sharp transition from elastic to plastic deformation.

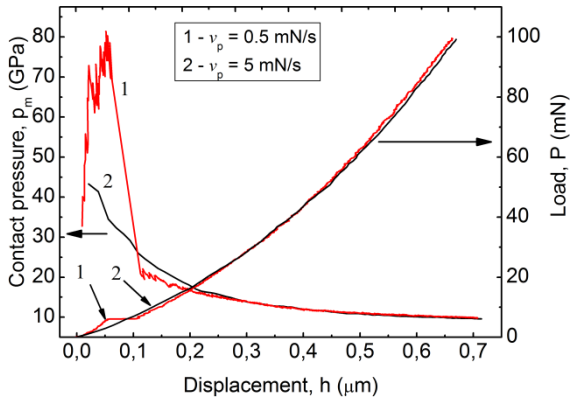

Fig. 7 Contact pressure versus penetration depth $p_m(h)$ dependences during loading for 100 mN indentations made at different loading rates: 0.5 and 5 mN/s, and respective *P(h)* curves

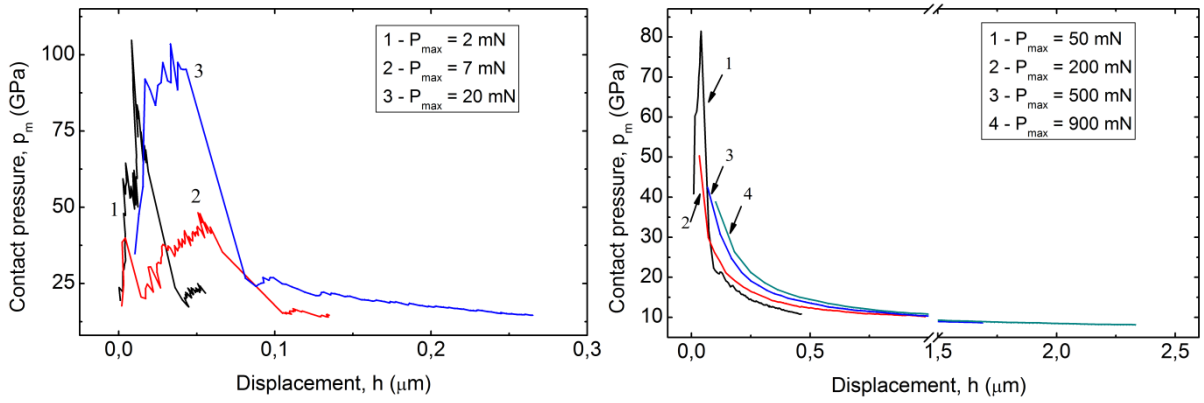

a **b**

Fig. 8 Contact pressure versus penetration depth dependences during loading for indentations made with different loads P_{max}. P_{max}, mN: a – 2, 7, 20; b – 50, 200, 500, 900

One more interesting result confirmed these considerations. One can see from Fig. 3 and 6, that the surges on the *dh/dt(h)* curves, caused by sharp increase of the strain rate during pop-ins, desappear with the increase of loading rate, just when the strain rates at the beginning of indenter penetration become higher than the strain rates during pop-ins. This means that just the velocity of dislocations, i.e. their kinetic energy has a determinant role in the elastic-to-plastic transition mechanism. The necessary kinetic energy for dislocation motion is induces by both macroscopisc strain rate and stresses, external and internal.

The above presented results allow asserting that the attenuation and disappearance of the pop-ins on the *P-h* curves with the increase of peak load (Fig. 4) is not related to the smearing of the effect due to the increased spatial resolution, but it is connected with the increase of loading and strain rate and the change of the elastic-to-plastic transition mechanism from sharp to gradual one.

A comparison of the patterns of dislocation rosettes around the imprints (Fig. 9) with the shape of the *P-h* curves shown in Fig. 1, 2 revealed new regularities that allow us to establish a certain hierarchy in the realization of deformation mechanisms in a wide range of loads under nanomicroindentation. As was shown above in Fig. 1, pop-in jumps were recorded on the *P-h* curves starting with the smallest load (P_{max} = 2 mN). Two small dislocation rosettes of approximately circular shape are visible for this load in Fig. 9. However, as follows from Fig. 1a, the first jump is formed at a load of $P_i \approx$ (0.2÷0.3) mN. The appearance of the first pop-in jump is due to the initial nucleation of dislocations in the process of nanoindentation.

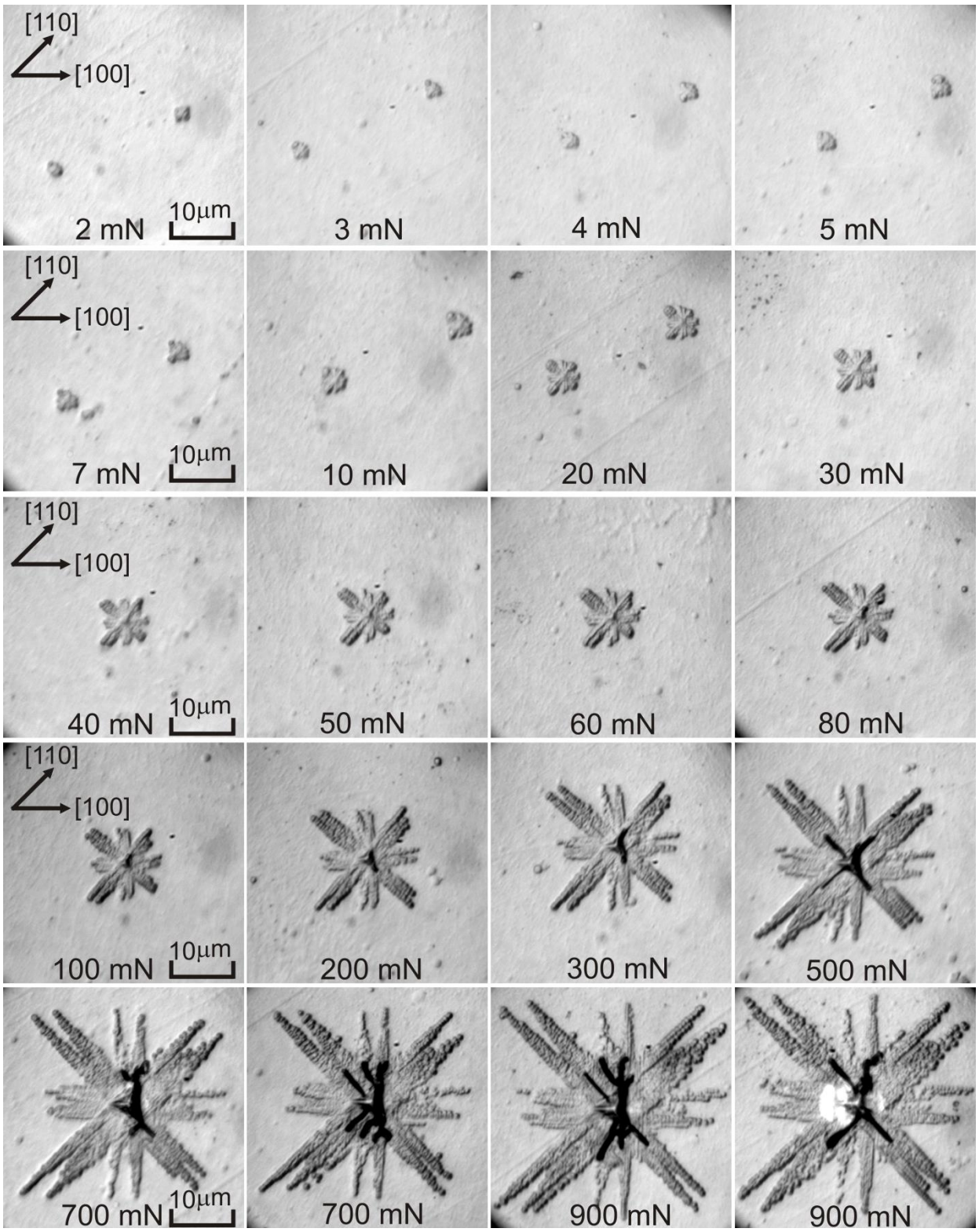

Fig. 9 Evolution of the dislocation rosettes near the imprints obtained as a result of dynamic nanomicroindentation by various loads in the interval P_{max} = (2÷900) mN

Therefore, it can be assumed that before the first jump, the elastic strain in the crystal predominates over the plastic deformation. With increasing the load value, the internal stresses in the zone under indenter reach critical values, that leads to plastic deformation with the appearance of initial dislocation loops under the imprints. The second pop-in jump occurs at P_i≈(1.4÷1.7) mN and is due to the

development of dislocation structure formed after the first pop-in jump (compare Fig.1a, the insert, with Fig. 9 (P_{max} =2÷4 mN)).

With the growth in the load in the range P_{max} =(5÷50) mN, the dislocation structures continue to develop, the edge and screw dislocation arms become more pronounced, and as a result, another pop-in jump appears at the *P-h* curves for P_i≈(4.5÷5.0) mN (Fig. 1a, b; 2 a-d). The formation of pop-in jumps is also reflected in the course of the hardness curve *H(P),* Fig. 10. Due to the facilitated translational slip of dislocations around the imprint, the hardness of MgO crystals decreases in the interval (P_i = (2÷50) mN) (stage I on the curve *H(P)*). In the scientific literature this stage is called ISE (Indentation Size Effect) [8,14, 20].

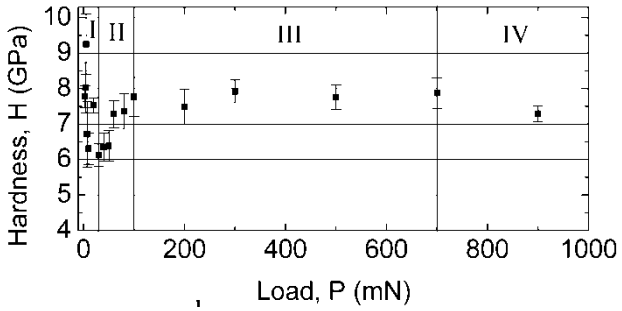

Fig. 10 The *H*(*P*) hardness-load dependence

As the load increases, (50÷100) mN, and correspondingly, the depth of the imprints grows, the dislocation structures become more complex (Fig. 9, 50÷100 mN). This increases the resistance of the material to the indenter penetration (the section of the curve *P(h),* loading step) and leads to an increase in *H* (stage II on the curve *H(P)*). With further increase in the load (P_{max} = (200÷700) mN), the hardness curve shows a saturation (stage III on the curve *H*(*P*)). In this interval, the dislocation rosettes actively develop, extend and expand due to the creation of multirow arms (Fig. 9, 200÷900 mN).

At this stage, the multiplication of dislocations takes place, the rosettes are formed from the dislocations located in all the active slip planes of the $\{110\}_{45}$ ($(110)_{45}$, $\left(\bar{1}\bar{1}0\right)_{45}$, $\left(\bar{1}10\right)_{45}$, $\left(1\bar{1}0\right)_{45}$, $\left(101\right)_{45}$, $\left(\bar{1}0\bar{1}\right)_{45}$, $\left(\bar{1}01\right)_{45}$, $\left(10\bar{1}\right)_{45}$) and $\{110\}_{90}$ ($(110)_{90}$, $\left(\bar{1}\bar{1}0\right)_{90}$, $\left(\bar{1}10\right)_{90}$, $\left(1\bar{1}0\right)_{90}$) type. All these slip planes intersect mutually and, respectively, dislocation loops located in these planes are also mutually intersected. This leads to the creation of very complex dislocation rosettes in which sedentary dislocations, dislocation walls and disclinations are formed. For this reason, the most complex dislocation-disclination reactions take place in the indentation zone, leading to the translation-rotation processes, fragmentation of the structure, the nanocracks creation and so on [45-48]. In the area under imprints the superhigh internal stresses are created, which are discharged due to the crack formation during the unloading stage.

The cracks are clearly visible in the center of the dislocation rosettes near the imprints at P_{max} = (80÷900) mN (Fig. 9). This process is recorded on the unloading part of *P-h* curves as pop-out jumps, that is, these cracks are of a relaxation nature. Along with this, the cracks may appear as well during loading for the loads P_{max}> 700 mN. It leads to a decrease in hardness and the appearance of a softening portion on the *H*(*P*) curve (step IV in Fig. 10).

The data presented above demonstrate the result of relaxation of the MgO single crystal during dynamic indentation by the formation of cracks and elastic-plastic reconstruction of the deformed zone. To confirm this statement, the images of imprints and the micro-relief near them are shown in Fig. 11 for loads P_{max} = (7÷40) mN. The images taken in the atomic force microscope indicate the displacement of the material to the surface with the formation of nanoscale hills of the material near the imprints (pile-up effect), mainly due to the slip of dislocations along the $\{110\}_{45}$ planes [45-49].

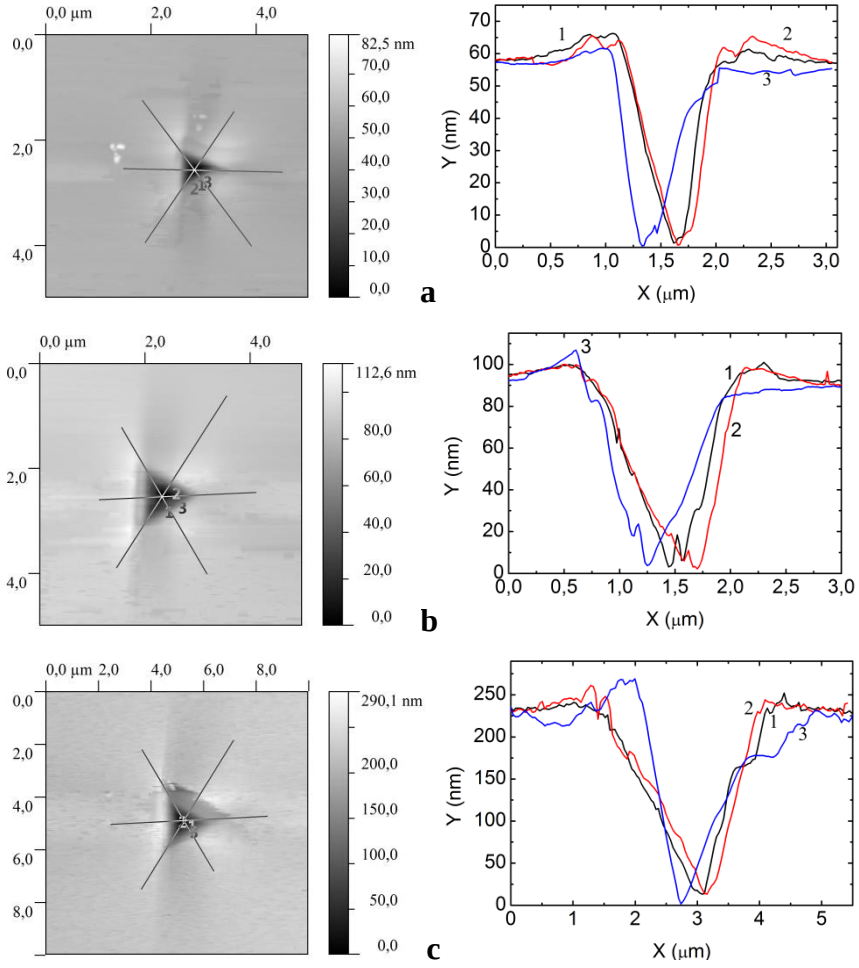

Fig. 11 AFM images of imprints and the micro-relief near them. P_{max}, mN: a – 7; b – 10; c – 40

The study of the imprint microstructure using the atomic force microscopy (AFM) showed that the relief of the material in the pile-up zone is not uniform, but it forms a wavy surface with oval bends, which becomes smoother by moving away from the sides of the imprints. It is known [50], that under the action of concentrated load the stresses in a given point of a solid can be described by the equation:

$$\sigma_r = (A \cos \theta) / r \qquad (7),$$

where θ and r are the polar coordinates of the given point with respect to the loading point, and A is a constant. According to equation 7, the stresses around the imprint decrease inverse proportionally to the distance from the applied load r. Therefore the displacement of material decreases gradually when moving away from the imprint that leads to the decrease of the height of the pile-ups and the diminution of the oval bends. Also it was observed that the surface of the imprints is not absolutely smooth. The irregularities in the form of small steps and facets are clearly seen on the cross section of the imprint surface (Fig. 11) and can be attributed to the development of the translation-rotation deformation. These facts together with several other results (reorientation bands, asterism of Laue spots, fragmentation) [45, 46, 48, 51-53] allowed us to conclude that the displacement of the material during indentation takes place through the dislocation-disclination deformation mechanism leading to rotational effects and intensive movement of material.

Conclusion

The instrumented nanomicroindentation of the (001) face of MgO single crystals under different loading rate and peak loads revealed different elastic-to-plastic transition: with pop-ins formation - a sharp mechanism, and without pop-ins formation – a gradual one. This difference was explained by different strain rate and kinetic energy of dislocations, the increase of which leads to the transition from the sharp to the gradual mechanism.

For the first time, three types of pop-in jumps were identified, as well as a serration effect, and the relationship between their appearance and the type of dislocation rosettes around the imprints was established. It is shown that the formation of pop-in jumps is due to various mechanisms of plastic deformation:

- 'pop-in'-1 – homogeneous nucleation of sliding dislocation loops near the imprint at the initial stages of indentation;
- 'pop-in'-2 – the development of dislocation structures around the imprints, the formation of edge and screw dislocation ~~beams~~ arms;
- 'pop-in'-3 – further development of the dislocation structures due to the deformation across all the active slip planes of the $\{110\}_{45}$ and $\{110\}_{90}$ type by the multiplication of dislocations.

With further growth of the load, the new deformation structures are formed under the imprints (sedentary dislocations, dislocation walls, disclinations, cracks, etc.). As a result, the translation-rotation mechanism of the deformation takes place on this stage of indentation. During the load removal, the relaxation processes cause the appearance of the pop-out jumps.

Acknowledgments

References

[1] Zhang T-Y, Xu W-H, Zhao M-H (2004) The role of plastic deformation of rough surfaces in the size-dependent hardness, Acta Mater 52:57-68.

[2] Tuck JR, Korsunsky AM, Bhat DG, Bull SJ (2001) Indentation hardness evaluation of cathodic arc deposited thin hard coatings, Surf Coat Tech 139:63-74.

[3] Gouldstone A, Van Vliet KJ, Suresh S (2001) Nanoindentation: Simulation of defect nucleation in a crystal, Nature London 411(6838):656-656.

[4] Lorenz D, Zeckzer A, Hilpert U, Grau P, Johansen H, Leipner HS (2003) Pop-in effect as homogeneous nucleation of dislocations during nanoindentation, Phys Rev B67:172101-1-4. doi: 10.1103/PhysRevB.67.172101.

[5] Tromas, J. Colin, C. Coupeau, J.C. Girard, J. Woirgard, and J. Grilhe. Pop-in phenomenon during nanoindentation in MgO. Eur. Phys. J. AP 8, 123{128 (1999).

[6] Alex Montagne 1, Vale´rie Audurier, Christophe Tromas. Influence of pre-existing dislocations on the pop-in phenomenon during nanoindentation in MgO. Acta Materialia 61 (2013) 4778–4786.

[7] J.E. Bradby, J.S. Williams, M.V. Swain. Pop-in events induced by spherical indentation in compound semiconductors. J. Mater. Res., Vol. 19, No. 1, Jan 2004, p. 380-386.

[8] Huang Y, Zhang F, Hwang KC, Nix WD, Pharr GM, Feng G (2006) A model of size effects in nanoindentation, J Mech Phys Solids 54:1668-1686.

[9] Chicot D (2009) Hardness length-scale factor to model nano- and micro-indentation size effects, Mater Sci Eng A 499:454–462.

[10] Korsunsky AM, Mc Gurk MR, Bull SJ, Page TF (1998) On the hardness of coated systems, Surf Coat Tech 99:171–183.

[11] Golovin YuI (2008) Nanoindentation and mechanical properties of solids in submicrovolumes, thin near-surface layers, and films: A Review, Phys Sol State 50(12): 2205-2236.

[12] Pharr GM, Oliver WC, Clarke DR (1990) The Mechanical Behavior of Silicon during Small-Scale Indentation, J Electron Mater 19(9):881–887.

[13] Ohmura T, Matsuoka S, Tanaka K, Yoshida T (2001) Nanoindentation load-displacemant behavior of pure face centered cubic metal thin films on a hard substrate, Thin Solid Films 385:198-204.

[14] Durst K, Backes B, Franke O, Göken M (2006) Indentation size effect in metallic materials: Modeling strengh from pop-in to macroscopic hardness using geometrically necessary dislocation, Acta Mater 54:2547-2555.

[15] Page TF, Oliver WC, Mc Hargue CJ (1992) The deformation behavior of ceramic crystals subjected to very low load (nano)indentations, J Mater Res 7:450-473.

[16] Bei H, Gao YF, Shim S, George EP, Pharr GM (2008) Strength differences arising from homogeneous versus heterogeneous dislocation nucleation, Phys Rev B 107:060103(R). doi:10.1103/PhysRevB.77.060103.

[17] Li J, Van Vliet KJ, Zhu T, Yip S, Suresh S (2002) Atomistic mechanisms governing elastic limit and incipient plasticity in crystals, Nature 418(6895):307-310. doi:10.1038/nature00865.

[18] Begau C, Hartmaier A, George EP, Pharr GM (2011) Atomistic processes of dislocation generation and plastic deformation during nanoindentation, Acta Mater 59:934-942.

[19] Šandera P, Pokluda, Schöber T, Hornikova J, Cerny M (2014) Modeling load-displacement curve and pop-in effect in nanoindentation tests, Procedia Mater Sci 3:1111-1116. doi: 10.1016/j.mspro.2014.06.181.

[20] Nix WD and Gao H (1998) Indentation size effects in crystalline materials: A law for strain gradient plasticity, J Mech Phys Solids 46(3):411-425.
[21] Leipner HS, Lorenz D, Zeckzer A, Grau P (2001) Dislocation-related pop-in effect in gallium arsenide, Phys Stat Sol (a) 183(2):R4-R6.
[22] Tromas C, Gaillard Y, Woirgard J (2006) Nucleation of dislocations during nanoindentation in MgO, Phil Mag 86:5595–5606.
[23] Grabco DZ, Pyrtsac KM, Shikimaka OA (2016) Mechanical properties of polycrystalline copper and single-crystal LiF initial components for composite system Cu/LiF, Surf Eng Appl Electrochem 52(3):233-241. doi:10.3103/S1068375516030066.
[24] Grabco DZ, Pyrtsak KM, Ghimpu LZ, Volodina GF (2016) Mechanical properties of the coating/substrate composite system: Nanostructured copper films on a LiF substrate, Surf Eng Appl Electrochem 52(4):319-333. doi:10.3103/S1068375516040074.
[25] Oliver WC and Pharr GM (1992) An improved technique for determining hardness and elastic modulus using load and displacement sensing indentation experiments, J Mater Res 7(6):1564-1583.
[26] Shikimaka O, Prisacaru A, Burlacu A (2015) Effect of long-term holding under contact loading on the specific features of phase changes in silicon, Mat Sci 51(3):405-411.
[27] Kiener D, Durst K, Rester M, Minor AM Revealing deformation mechanisms with nanoindentation (2009) JOM (The Journal of the Minerals, Metals & Materials Society) 61(3) 14-23. https://doi.org/10.1007/s11837-009-0036-4
[28] Beegan D, Chowdhury S, Laugier MT (2004) The nanoindentation behaviour of hard and soft films on silicon substrates, Thin Solid Films 466:167–174.
[29] Soer WA, De Hosson JTM, Minor AM, Morris JW, Stach EA (2004) Effect of solute Mg on grain boundary and dislocation dynamics during nanoindentation of Al-Mg thin films, Acta Mater 52:5783–5790.
[30] Wang F, Xu K (2004) An investigation of nanoindentation creep in polycrystalline Cu thin film, Mater Lett 58:2345–2349. doi 10.1016/j.matlet.2004.02.043.
[31] Croitor L, Coropceanu EB, Chisca D, Baca SG, J van Leusen, Kögerler P, Bourosh P, Kravtsov VCh, Grabco D, Pyrtsac C, Fonari MS (2014) Effects of anion and bipyridyl bridging ligand identity on the Co(II) coordination networks, Cryst Growth Des 14:3015–3025. doi 10.1021/cg500646r.
[32] Grabco D, Shikimaka O, Elisa M, Sava B, Boroica L, Harea E, Pirtsac C, Prisacaru A, Feraru I, Ursu D (2012) The surface morphology and strength properties of SiO_2–P_2O_5–Nd_2O_3 glassy films, Surf Eng Appl Electrochem, 48(5):430–438.
[33] Grabco D, Harea E, Shikimaka O, Sherban D (2012) Elastoplastic response of TCO/Si coated systems to local loading. In: Reimer A (ed) Horizons in world physics. Huntington NY: Nova Sci, 277(4):111–131.
[34] Golovin YuI, Vasyukov VM, Korenkov VV, Stolyarov RA, Shuklinov AV, Polyakov LE (2011) Size Effects in the Hardness of FCC Metals on Micro and Nanoscales, Tech Phys 56(5):642-645.
[35] Zuev LB, Barannikova SA, Zarikovskaya NV, Zykov IYu (2001) Phenomenology of wave processes in a localized plastic flow, Phys Solid State 43:1483-1487.
[36] Suresh S, Nieh TG, Choi BW (1999) Nano-indentation of copper thin films on silicon substrate, Scr Mater 41:951–957.
[37] Pharr GM, Oliver WC, Clarke DR (1990) The mechanical behavior of silicon during small-scale indentation, J Electron Mater 19:881-887.

[38] Chang L and Zhang LC (2009) Deformation mechanisms at pop-out in monocrystalline silicon under nanoindentation, Acta Mater 57:2148–2153.
[39] Lawn R (1998) Indentation of ceramics with spheres: a century after Hertz, J Amer Ceram Soc 81:1977–1994.
[40] Orowan E (1948) Symposium on internal stresses in metals and alloys. Institute of Metals, London 451-454.
[41] Frank FC (1949) On the Equations of Motion of Crystal Dislocations, Proc. Phys. Soc. A 62(2):131-134 https://doi.org/10.1088/0370-1298/62/2/307.
[42] Альшиц ВИ, Инденбом ВЛ (1975) Динамическое торможение дислокаций, Успехи физических наук 115(1):3-39 // Al'shits VI, Indenbom VL (1975) Dynamic braking of dislocations, Physics-Uspekhi (Advances in Physical Sciences) 115(1):3-39.
[43] Dislocations in Solids (2004) Nabarro FRN, Hirth JP (eds) Elsevier B V 12(70).
[44] Новиков НВ, Дуб СН, Мильман ЮВ, Гриднева ИВ, Чугунова СИ (1996) Применение метода наноиндентирования для изучения фазового превращения полупроводник—металл в кремнии, Сверхтвердые материалы 3: 36 – 45 // Novikov NV, Dub SN, Milman YV, Gridneva IV, Chugunova SI (1996) Application of the nanoindentation method for studying the semiconductor-metal phase transition in silicon, J Superhard Mater 3: 36 – 45.
[45] Grabco D, Pushcash B, Dyntu M, Shikimaka O (2002) Thermal evolution of deformation zones around microindentations in different types of crystal, Phil Mag A 82(10):2207-2215.
[46] Grabco D (2002) Dislocation-disclination mechanism of deformation under microindentation, Moldavian Journal of the Physical Sciences (MJPS) 1(3):94-103.
[47] Chaudhri MM (2004) Dislocations and indentations. In: Nabarro FRN, Hirth JP (eds) Dislocation in Solids, Elsevier 12(70):449-550.
[48] Боярская ЮС, Грабко ДЗ, Кац МС (1986) Физика процессов микроиндентирования. Кишинев Штиинца // Boyarskaya YuS, Grabco DZ, Kats MS (1986) Physics of microindentation processes, Chisinau, Shtiintsa.
[49] Boyarskaya YuS, Grabco DZ (1973) Some Features of plastic deformation of LiF and NaCl single crystals at high temperatures, Kristall und Technik 8(12):1367-1377.
[50] Frocht MM (1948) Photoelasticity, v.II, Publ. John Wiley & Sons 28:32-79.
[51] Shikimaka O, Grabco D (2008) Deformation created by Berkovich and Vickers indenters and its influence on surface morphology of indentations for LiF and CaF_2 single crystals, J Phys D Appl Phys 41:074012 (6pp).
[52] Grabco D, Shikimaka O, Harea E (2008) Translation-rotation plasticity as basic mechanism of plastic deformation in macro-, micro- and nanoindentation processes, J Phys D Appl Phys 41:074016 (9pp).
[53] Грабко ДЗ, Лавровская НА, Мединская МИ (1991) Закономерности деформирования и разрушения при локальном нагружении ионных кристаллов, Латвийский журнал физических и технических наук 5:72-80 // Grabco DZ, Lavrovskaya NA, Medinskaya MM (1991) Regularities of deformation and fracture at local loading of ionic crystals, Latvian Journal of Physics and Technical Sciences 5:72-80.